TASK QUARTERLY 7 No 4 (2003), 701–721

MODELLING OF SILO DISCHARGE AND FILLING PROBLEMS BY THE MATERIAL POINT METHOD

ZDZISŁAW WIĘCKOWSKI

Technical University of Łódź, Chair of Mechanics of Materials,
Al. Politechniki 6, 93-590 Łódź, Poland
zwi@p.lodz.pl

(Received 2 June 2003)

Abstract: The problems of flow of a granular material in the processes of silo discharge and filling are considered. Dynamic, two-dimensional problems are analyzed, both the plane and axisymmetric ones. The material point method is applied as a tool of analysis, a variant of the finite element method capable of solving pertinent equations of motion on an arbitrary computational element mesh and tracing state variables at material points chosen independently of the mesh. The mechanical behaviour of a granular material is described with non-associative elastic-perfectly plastic and elastic-viscoplastic material models with the Drucker-Prager yield condition. The influence of friction between the flowing granular body and silo walls is taken into account. The material point method enables one to analyze silos of arbitrary shapes, including silos with inserts controlling the flow of the stored material. The mass and funnel types of flows are analyzed.

Keywords: granular flow, plasticity, viscoplasticity, finite element method, material point method

1. Introduction

The problems of flow of a granular material while discharging or filling a silo is interesting not only for its designer, who should calculate interactions between the flowing material and silo walls, but also for its user, who should be able to predict the flow pattern and rate.

Due to the complexity of the problem, various simplifications have been made in the analysis of such processes to estimate wall tractions and flow patterns for the flowing material. Since the eighties of the previous century some researchers have been applying various numerical approaches in order to solve this problem properly formulated from the view-point of continuum mechanics. Eibl, Häussler and Rombach have solved the problem of silo discharge using the finite element method [1, 2]. They have used the Eulerian description of motion in their analysis and treated the flowing granular material as a fluid. Such an approach is very useful when the region occupied by the flowing material is constant in time, *i.e.* when the silo is continuously refilled. This approach has also been applied by other researchers [3, 4]. However, the finite element method formulated in the Lagrangian description of motion is useful when the

entire process of silo discharge is analyzed. This approach, with mesh-rezoning applied in order to restore the proper shapes of elements subjected to large distortions, has been presented in [5]. The entire process of silo discharge and filling can be solved by the discrete element method [6–8], in which the granular material is treated as a set of balls or cylinders, usually of equal diameters. It seems, however, that applicability of this method is limited to the case when the ratio between the diameters of the silo outlet and grain is not very large. In order to eliminate the disadvantages of the Lagrangian approach to the finite element method due to large element distortions, the material point method has been applied to the silo discharge problem by the author of the present paper and his co-workers [9], and recently by Oger *et al.* [10] and Mühlhaus *et al.* [8].

As mentioned above, the material point method (MPM) is utilized in the analysis of the considered problems of discharging and filling a silo. The method, originally introduced in fluid dynamics by Harlow and co-workers (see [11] and references therein) and known as the particle-in-cell (PIC) method, has been applied successfully to the problems of solid mechanics by Burgess, Sulsky, Brackbill, Chen, Schreyer and Zhou [12–15]. The material point method may be regarded as the finite element method formulated in an arbitrary Lagrangian-Eulerian description of motion. State variables for the analyzed body are traced at a set of points (material points) defined independently of the Eulerian mesh (computational mesh) on which the equations of motion are formulated and solved. As the computational mesh can be defined in an arbitrary way, the problem of mesh distortion, which leads to difficulties in the Lagrangian formulation, is thus avoided. The material point method can be classified as a point-based method, or a meshless method. An overview of point-based methods can be found in an article by Belytschko *et al.* [16] and books by Zienkiewicz and Taylor [17] and Liu [18].

2. Setting the problem

Let us consider a time interval $I=[0,T]$, where $T>0$. Let $\Omega\subset\mathcal{R}^3$ denote the region occupied by the body at time $t\in I$, the boundary, $\partial\Omega$, of which consists of three parts, Γ_u, Γ_σ and Γ_c, such that:

$$\overline{\Gamma_u}\cup\overline{\Gamma_\sigma}\cup\overline{\Gamma_c}=\partial\Omega, \qquad \Gamma_u\cap\Gamma_\sigma=\Gamma_u\cap\Gamma_c=\Gamma_c\cap\Gamma_\sigma=\emptyset.$$

Although two-dimensional problems are solved in the paper, the general three-dimensional case is considered in this section.

The solution to the problem satisfies the governing relations described in the subsections below.

2.1. Equations of motion

The equations of motion are as follows:

$$\sigma_{ij,j}+\varrho b_i-\varrho a_i=0 \quad \text{on } \Omega,$$

where σ_{ij} denotes the Cauchy stress tensor, ϱ is mass density, and b_i and a_i are vectors of body forces and acceleration, respectively.

2.2. Boundary conditions

It is assumed that the displacements are given on boundary part Γ_u:

$$u_i = U_i \quad \text{on } \Gamma_u,$$

and stresses are known on boundary part Γ_σ:

$$\sigma_{ji} n_j = t_i \quad \text{on } \Gamma_\sigma,$$

where t_i is the Cauchy stress vector, and n_i denotes the unit vector outwardly normal to the boundary, $\partial\Omega$.

2.3. Frictional contact conditions

The conditions of unilateral frictional contact are considered on boundary part Γ_c. Let $g_N(\mathbf{x})$, where $\mathbf{x} \in \Gamma_c$, denote a distance function defined as the distance between the considered point of the surface and the closest point on the surface of an obstacle body being or likely to come into contact with point $\mathbf{x}$. The frictional contact conditions can be described by the following set of relations:

$$\begin{aligned} g_N \geq 0, \qquad \sigma_N \leq 0, \qquad \dot{u}_N \sigma_N = 0, \\ f_c(\sigma_N, \boldsymbol{\sigma}_T) \leq 0, \qquad \dot{u}_{Ti} \sigma_{Ti} \leq 0, \end{aligned} \tag{1}$$

where the Coulomb friction condition is applied:

$$f_c(\sigma_N, \boldsymbol{\sigma}_T) = -\mu|\sigma_N| + \|\boldsymbol{\sigma}_T\| \leq 0, \tag{2}$$

wherein σ_N and $\boldsymbol{\sigma}_T$ denote the normal and tangential components of the Cauchy stress vector, respectively, $\sigma_N = \sigma_{ij} n_i n_j$, $\sigma_{Ti} = \sigma_{kj} n_k (\delta_{ij} - n_i n_j)$, μ is the friction coefficient, u_N and $\mathbf{u}_T$ are the normal and tangential components of the displacement vector, respectively, and $\|\cdot\|$ denotes the Euclidean norm of a vector.

The variational formulation of the contact problem for deformable bodies leads to an implicit variational inequality, some terms of which are non-differentiable functionals (see *e.g.* [19, 20]), which makes the problem difficult to solve. To overcome these difficulties, the penalty regularization method is used for the frictional constraints (1) and (2).

In a regularized form of the contact law, the relation between the normal components of stress rate and relative velocity has the form:

$$\dot{\sigma}_N = \begin{cases} -c_N \dot{u}_N & \text{if } g_N \leq 0, \\ 0 & \text{if } g_N > 0. \end{cases} \tag{3}$$

The tangential component of relative velocity (slip) is expressed as sum of two parts $\dot{\mathbf{u}}_T^{\mathrm{e}}$ and $\dot{\mathbf{u}}_T^{\mathrm{i}}$, respectively called elastic and inelastic, which satisfy relations similar to the constitutive relations for an elastic-plastic material (*e.g.* [21, 22]):

$$\dot{u}_{Ti}^{\mathrm{e}} = -\frac{1}{c_T} \dot{\sigma}_{Ti}, \tag{4}$$

$$\dot{u}_{Ti}^{\mathrm{i}} = \begin{cases} -\dot{\lambda} \dfrac{\partial f}{\partial \sigma_{Ti}} & \text{if } f(\sigma_N, \boldsymbol{\sigma}_T) = 0, \\ 0 & \text{if } f(\sigma_N, \boldsymbol{\sigma}_T) < 0, \end{cases} \tag{5}$$

where $\dot{\lambda} \geq 0$, c_N and c_T are penalty parameters.

2.4. Initial conditions

The following initial conditions are considered:

$$u_i(0) = u_i^0, \qquad \dot{u}_i(0) = v_i^0, \qquad \sigma_{ij}(0) = \sigma_{ij}^0,$$

where u_i^0, v_i^0 and σ_{ij}^0 denote the initial fields of displacements, velocities and stresses, respectively.

2.5. Constitutive relations

Several constitutive models based on the concepts of plasticity and hypoplasticity are applied to describe the mechanical behaviour of granular materials.

In the analysis of the discharge problem, non-associative elastic-perfectly plastic and elastic-viscoplastic material models with the Drucker-Prager yield condition are applied. The third model used in discharge modelling is the hypoplastic model introduced by Kolymbas. Let B denote a convex set of plastically admissible stresses:

$$B = \{\tau_{ij}: \quad f(\tau_{ij}) \leq 0\},$$

where the yield condition has the following form:

$$f(\sigma_{ij}) = q - mp.$$

In the above relation, parameter $m = 18\sin\varphi/(9 - \sin^2\varphi)$ depends on the angle of internal friction, φ, and p and q are stress invariants defined as follows:

$$p = -\frac{1}{3}\sigma_{ii}, \qquad q = \sqrt{\frac{3}{2}s_{ij}s_{ij}},$$

where $s_{ij} \equiv \sigma_{ij} + p\delta_{ij}$ denotes the deviatoric part of the stress tensor.

The constitutive relations for the Drucker-Prager elastic-perfectly plastic model can be written in the following form:

$$d_{ij} = d_{ij}^{\mathrm{e}} + d_{ij}^{\mathrm{p}}, \tag{6}$$

$$d_{kl}^{\mathrm{e}} = D_{ijkl}^{-1}\overset{\nabla}{\sigma}_{ij}, \tag{7}$$

$$d_{ij}^{\mathrm{p}} = \begin{cases} \dot{\lambda}\dfrac{\partial g}{\partial \sigma_{ij}} & \text{if } f(\sigma_{ij}) = 0, \\ 0 & \text{if } f(\sigma_{ij}) < 0, \end{cases} \tag{8}$$

where $\dot{\lambda} \geq 0$, and g denotes the plastic potential defined by the relation $g = q$, which means that the material is plastically incompressible. The following notation has been used above: $d_{ij} = \frac{1}{2}(\dot{u}_{i,j} + \dot{u}_{j,i})$ is the tensor of deformation rate; d_{ij}^{e} and d_{ij}^{p} are its elastic and plastic parts, respectively;

$$\overset{\nabla}{\sigma}_{ij} = \dot{\sigma}_{ij} - \sigma_{ik}\dot{\omega}_{kj} - \sigma_{jk}\dot{\omega}_{ki} \tag{9}$$

is the Jaumann stress rate tensor; $\dot{\omega}_{ij} = \frac{1}{2}(\dot{u}_{j,i} - \dot{u}_{i,j})$ denotes the spin tensor; and

$$D_{ijkl} = \frac{E}{1+\nu}\left(\frac{\nu}{1-2\nu}\delta_{ij}\delta_{kl} + \frac{1}{2}(\delta_{ik}\delta_{jl} + \delta_{il}\delta_{jk})\right)$$

is the tensor of elastic constants, where E and ν denote the Young modulus and Poisson ratio, respectively.

For the elastic-viscoplastic model, Equations (6)–(8) are replaced by the following ones:

$$d_{ij} = d^{\mathrm{e}}_{ij} + d^{\mathrm{vp}}_{ij}, \tag{10}$$

$$d^{\mathrm{e}}_{kl} = D^{-1}_{ijkl} \overset{\nabla}{\sigma}_{ij}, \tag{11}$$

$$d^{\mathrm{vp}}_{ij} = \gamma \langle \Phi(f) \rangle \frac{\partial g}{\partial \sigma_{ij}}. \tag{12}$$

The Φ function is chosen as follows:

$$\Phi(f(\sigma_{ij})) = \left(\frac{q - mp}{mp} \right)^N, \qquad N > 0. \tag{13}$$

γ denotes the viscosity coefficient, and the meaning of parentheses $\langle\rangle$ is defined by the following rule:

$$\langle \Phi(x) \rangle = \begin{cases} \Phi(x) & \text{if } x > 0, \\ 0 & \text{if } x \leq 0. \end{cases}$$

The third material model, applied to the filling problem, consists of two constitutive concepts. The relation between the average normal stress (pressure, $p = -\sigma_{ii}/3$) and volume change is described as per the Voigt model of a viscoelastic body, while for the relation between the deviatoric parts of the stress tensor and the tensor of deformation rate, the model of an elastic-viscoplastic body is employed. For the non-cohesive material considered in the analysis, the relation between pressure and volume change can be written in the following form:

$$p = p_0 \exp \left[\frac{1 + e_0}{\kappa} (1 - \exp \varepsilon_{\mathrm{vol}}) \right] + \langle -\mu \dot{\varepsilon}_{\mathrm{vol}} \rangle, \tag{14}$$

where p_0 and e_0 denote the pressure and void ratios for the state with respect to which the volume change is measured, κ – the elastic coefficient, μ – the bulk viscosity ratio, the dot – the time derivative, and the brackets, $\langle\rangle$, indicate the positive part of an expression, $\langle x \rangle = \max(0, x)$. The elastic part of pressure, p, (the first component of the right-hand side in Equation (14)) follows from the linear relation between the void ratio and pressure, well-known in soil mechanics (see *e.g.* [23]):

$$e - e_0 = -\kappa \ln \frac{p}{p_0}.$$

Let s_{ij} and e_{ij} denote the deviatoric parts of the stress tensor, σ_{ij}, and the tensor of deformation rate, d_{ij},

$$s_{ij} = \sigma_{ij} + p\delta_{ij}, \qquad e_{ij} = d_{ij} - \frac{1}{3} d_{kk} \delta_{ij}.$$

The Drucker-Prager yield condition is applied in the formulation of constitutive relation for the deviatoric tensors. Using additive decomposition for the rate-of-deformation tensor, $e_{ij} = e^{\mathrm{e}}_{ij} + e^{\mathrm{vp}}_{ij}$ (where e^{e}_{ij} and e^{vp}_{ij} are the elastic and viscoplastic parts, respectively), the constitutive relation can be written in the following form:

$$e^{\mathrm{e}}_{ij} = \frac{1}{G} \overset{\nabla}{s}_{ij}, \qquad e^{\mathrm{vp}}_{ij} = \gamma \langle \Phi(f) \rangle \frac{\partial g}{\partial s_{ij}}, \tag{15}$$

where $\overset{\nabla}{s}_{ij}$ is the Jaumann-Zaremba measure of the stress rate tensor, and G denotes the shear modulus dependent on pressure, p, and Poisson's ratio, ν:

$$G = \frac{3}{2}\frac{1-2\nu}{1+\nu}\frac{1+e_0}{\kappa}p\exp\varepsilon_{\mathrm{vol}}.$$

The following non-associated flow rule is assumed in Equation (15): $g = q$, which means that the material is plastically incompressible. The Φ function is chosen as in the model described previously (Equation (13)).

In the analysis of the discharge problem, one more constitutive model is utilized, *viz.* the hypoplastic model described by Kolymbas [24, 25]. The constitutive relation has the following form:

$$\overset{\nabla}{\sigma}_{ij} = C_1\frac{1}{2}(\sigma_{ik}d_{kj} + d_{ik}\sigma_{kj}) + C_2\sigma_{kl}d_{kl}\delta_{ij} + \left(C_3\sigma_{ij} + C_4\frac{\sigma_{iq}\sigma_{qj}}{\sigma_{pp}}\right)\sqrt{d_{kl}d_{kl}}, \qquad (16)$$

where $C_1,\ldots,C_4$ are dimensionless constants determined in the three-axial compression test.

3. Material point solution

3.1. Space discretization

As in the standard finite element method, the equation of virtual work is used as the starting point for the formulation of the material point method:

$$\int_\Omega \varrho(a_i w_i + \frac{1}{\varrho}\sigma_{ij}w_{i,j})\mathrm{d}x = \int_\Omega \varrho b_i w_i \mathrm{d}x + \int_{\Gamma_\sigma} t_i w_i \mathrm{d}s + \int_{\Gamma_c}\sigma_{ij}n_j w_i \mathrm{d}s, \qquad \forall \mathbf{w}\in V_0, \quad (17)$$

where $V_0 = \{\mathbf{w}\colon\ w_i = 0 \text{ on } \Gamma_u\}$ denotes the space of displacement fields satisfying the homogeneous boundary conditions which are sufficiently regular in the sense of all mathematical operations required.

Two kinds of space discretization are used in the material point method. Firstly, the initial configuration of the analyzed body is divided into a finite number of subregions. Each of these subregions is represented by one of its points, called a material point. It is assumed that the whole mass of the specific subregion is concentrated at its corresponding material point, so that the mass density field may be expressed as follows:

$$\varrho(\mathbf{x}) = \sum_{P=1}^{N} M_P\delta(\mathbf{x}-\mathbf{X}_P), \qquad (18)$$

where M_P and $\mathbf{X}_P$ are mass and position of the P^{th} material point, respectively, $\delta(\mathbf{x})$ denotes the Dirac delta function, and N is the number of material points. At the same time, the equation of virtual work is formulated and solved in the Eulerian frame by the use of a computational mesh. This mesh can be chosen arbitrarily, which implies that the problem of mesh distortion does not occur in this formulation. An example of space discretization used in the material point method is shown in Figure 1.

Using Equation (18), we can write the equation of virtual work in the following form:

$$\sum_{P=1}^{N} M_P\left(a_i(\mathbf{X}_P)w_i(\mathbf{X}_P) + \sigma^{\varrho}_{ij}(\mathbf{X}_P)w_{i,j}(\mathbf{X}_P)\right) =$$

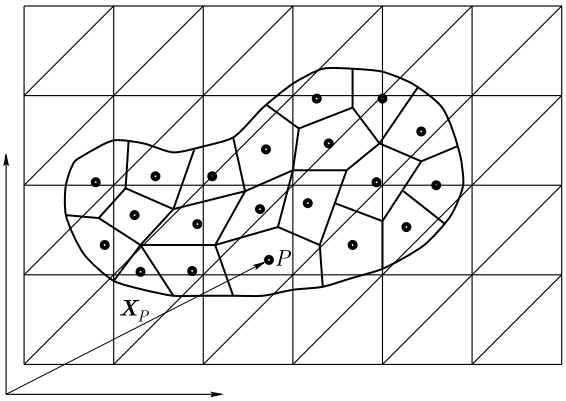

Figure 1. Space discretization: material points and computational mesh

$$\sum_{P=1}^{N} M_P b_i(\mathbf{X}_P) w_i(\mathbf{X}_P) + \int_{\Gamma_\sigma} t_i w_i \mathrm{d}s + \int_{\Gamma_c} \sigma_{ij} n_j w_i \mathrm{d}s, \tag{19}$$

where $\sigma_{ij}^{\varrho} = \sigma_{ij}/\varrho$. The same equation of virtual work can be obtained in the case of the axisymmetric problem if the field of mass density is represented as $\varrho(\mathbf{x}) = \sum_{P=1}^{N} M_P/(2\pi x)\delta(\mathbf{x}-\mathbf{X}_P)$, where variables (x,y,Θ) are used instead of (r,z,Θ).

The fields a_i and w_i are approximated as follows (the two-dimensional case is considered):

$$\mathbf{a}(\mathbf{x},t) \equiv \begin{bmatrix} a_x \\ a_y \end{bmatrix} = \mathbf{N}\mathbf{a}, \qquad \mathbf{w}(\mathbf{x},t) \equiv \begin{bmatrix} w_x \\ w_y \end{bmatrix} = \mathbf{N}\mathbf{w}, \tag{20}$$

where $\mathbf{N}$ is the matrix of global shape functions defined for the whole computational mesh,

$$\mathbf{N}(\mathbf{x}) = \begin{bmatrix} N_1(\mathbf{x}) & 0 & N_2(\mathbf{x}) & 0 & \ldots & N_n(\mathbf{x}) & 0 \\ 0 & N_1(\mathbf{x}) & 0 & N_2(\mathbf{x}) & \ldots & 0 & N_n(\mathbf{x}) \end{bmatrix},$$

$$\mathbf{a} = [a_{1x} \quad a_{1y} \quad a_{2x} \quad \ldots \quad a_{nx} \quad a_{ny}]^{\mathrm{T}}$$

and

$$\mathbf{w} = [w_{1x} \quad w_{1y} \quad w_{2x} \quad \ldots \quad w_{nx} \quad w_{ny}]^{\mathrm{T}}$$

are nodal values of fields a_i and w_i, respectively, and n denotes the number of nodes in the computational grid.

Let us define the following vectors for two-dimensional problems:

$$\mathbf{s}^{\varrho} = \frac{1}{\varrho} \begin{bmatrix} \sigma_{xx} \\ \sigma_{yy} \\ \sigma_{xy} \\ \hline \sigma_{\Theta\Theta} \end{bmatrix}, \qquad \mathbf{b} = \begin{bmatrix} b_x \\ b_y \end{bmatrix}, \qquad \mathbf{t} = \begin{bmatrix} t_x \\ t_y \end{bmatrix},$$

where the last term of vector $\mathbf{s}^{\varrho}$ corresponds to the axisymmetric problem. Using relations (20) in (19), we can rewrite the problem in the following discretized form:

$$\mathbf{w}^{\mathrm{T}} \sum_{P=1}^{N} M_P \mathbf{N}^{\mathrm{T}}(\mathbf{X}_P)\mathbf{N}(\mathbf{X}_P)\mathbf{a} + \mathbf{w}^{\mathrm{T}} \sum_{P=1}^{N} M_P \mathbf{B}^{\mathrm{T}}(\mathbf{X}_P)\mathbf{s}^{\varrho}(\mathbf{X}_P) =$$

$$\mathbf{w}^{\mathrm{T}}\sum_{P=1}^{N} M_P\mathbf{N}^{\mathrm{T}}(\mathbf{X}_P)\mathbf{b}(\mathbf{X}_P)+\mathbf{w}^{\mathrm{T}}\int_{\Gamma_\sigma}\mathbf{N}^{\mathrm{T}}\mathbf{t}\,\mathrm{d}s+\mathbf{w}^{\mathrm{T}}\mathbf{F}_c.$$

As vector $\mathbf{w}$ is arbitrary (except for the degrees of freedom defined at the nodes belonging to Γ_u), we obtain the following system of equations:

$$\mathbf{Ma}=\mathbf{F}+\mathbf{F}_c-\mathbf{R}, \tag{21}$$

where

$$\begin{aligned}\mathbf{M}&=\sum_{P=1}^{N} M_P\mathbf{N}^{\mathrm{T}}(\mathbf{X}_P)\mathbf{N}(\mathbf{X}_P),\\ \mathbf{F}&=\sum_{P=1}^{N} M_P\mathbf{N}^{\mathrm{T}}(\mathbf{X}_P)\mathbf{b}(\mathbf{X}_P)+\int_{\Gamma_\sigma}\mathbf{N}^{\mathrm{T}}\mathbf{t}\,\mathrm{d}s,\\ \mathbf{R}&=\sum_{P=1}^{N} M_P\mathbf{B}^{\mathrm{T}}(\mathbf{X}_P)\mathbf{s}^{\varrho}(\mathbf{X}_P),\end{aligned} \tag{22}$$

and the definition of contact forces follows from the relation:

$$\mathbf{w}^{\mathrm{T}}\mathbf{F}_c=\int_{\Gamma_c}\sigma_{ij}n_jw_i\,\mathrm{d}s.$$

Matrix $\mathbf{B}$ has the same structure as the strain-displacement matrix used in the standard finite element method:

$$\mathbf{B}(\mathbf{X}_P)=\left[\begin{array}{cccc|c}\dfrac{\partial N_1}{\partial x}(\mathbf{X}_P) & 0 & \dfrac{\partial N_2}{\partial x}(\mathbf{X}_P) & 0 & \ldots\\ 0 & \dfrac{\partial N_1}{\partial y}(\mathbf{X}_P) & 0 & \dfrac{\partial N_2}{\partial y}(\mathbf{X}_P) & \ldots\\ \dfrac{\partial N_1}{\partial y}(\mathbf{X}_P) & \dfrac{\partial N_1}{\partial x}(\mathbf{X}_P) & \dfrac{\partial N_2}{\partial y}(\mathbf{X}_P) & \dfrac{\partial N_2}{\partial x}(\mathbf{X}_P) & \ldots\\ \hline \dfrac{N_1}{x}(\mathbf{X}_P) & 0 & \dfrac{N_2}{x}(\mathbf{X}_P) & 0 & \ldots\end{array}\right]$$

where the last row exists in the case of the axisymmetric problem.

Because of the Dirac delta-function representation of mass density, Equation (18), the mass matrix is singular when its consistent form is considered. To solve system (21), a diagonalized matrix, $\mathbf{M}_l$, or a nearly consistent matrix, $\mathbf{M}_\alpha=\alpha\mathbf{M}+(1-\alpha)\mathbf{M}_l$, can be used instead of $\mathbf{M}$ where $0\le\alpha<1$ [12]. A diagonalized matrix, calculated by summing all terms in rows, is employed in this paper where triangular elements with linear shape functions are used.

3.2. Time integration of the dynamic problem

The solution to the dynamic system (21) is found for a discrete set of instants $t_1,t_2,\ldots,t_k,\ldots\in I$ $(0<t_1<t_2<\ldots<t_k\ldots<T)$ according to the explicit time integration procedure. For each time increment, the calculations consist of two steps: a Lagrangian step and a convective one.

In the Lagrangian step, the calculations are performed in a way similar to that of the updated Lagrangian formulation of the standard finite element method; it is

assumed that the computational mesh deforms together with the considered body. The state variables are calculated for each material point with shape functions and nodal parameters defined on the computational mesh. For example, the velocity vector for the Pth material point, $\mathbf{V}_P \equiv [V_{Px} \quad V_{Py}]^{\mathrm{T}}$, is obtained from the equation:

$$\mathbf{V}_P = \mathbf{N}(\mathbf{X}_P)\mathbf{v}^{\mathrm{e}},$$

where $\mathbf{v}^{\mathrm{e}} = [v_{1x} \quad v_{1y} \quad v_{2x} \quad v_{2y} \quad \ldots \quad v_{n_e x} \quad v_{n_e y}]^{\mathrm{T}}$ is the vector of nodal velocities of the element which the material point belongs to. The vector of the strain increment can be calculated using matrix $\mathbf{B}$ as follows:

$$\Delta\mathbf{e} = \Delta t \mathbf{B}(\mathbf{X}_P)\mathbf{v}^{\mathrm{e}},$$

where $\Delta\mathbf{e} = \Delta t[d_{xx} \quad d_{yy} \quad d_{xy}]^{\mathrm{T}}$ or $\Delta\mathbf{e} = \Delta t[d_{xx} \quad d_{yy} \quad d_{xy} \quad d_{\Theta\Theta}]^{\mathrm{T}}$ for the plane strain and axisymmetric problems, respectively. Then, the stresses can be obtained from the constitutive relations.

The convective step consists of mapping the velocity field from material points to the computational grid, which can remain in the same position as at the beginning of the time increment or can be changed. Nodal velocities, $\mathbf{v} = [v_{1x} \quad v_{1y} \quad v_{2x} \quad v_{2y} \quad \ldots \quad v_{nx} \quad v_{ny}]^{\mathrm{T}}$, are calculated from the following equation [12–15]:

$$\mathbf{M}\mathbf{v} = \mathbf{S}^{\mathrm{T}}\mathbf{M}_d\mathbf{V}, \tag{23}$$

which expresses the equivalence of momentum calculated for material points and for the computational grid, where $\mathbf{V} = [V_{1x} \quad V_{1y} \quad V_{2x} \quad V_{2y} \quad \ldots \quad V_{Nx} \quad V_{Ny}]^{\mathrm{T}}$ is the vector of velocities of all the material points, and matrices $\mathbf{S}$ and $\mathbf{M}_d$ are defined as follows:

$$\mathbf{S} = \begin{bmatrix} \mathbf{N}(\mathbf{X}_1) \\ \mathbf{N}(\mathbf{X}_2) \\ \vdots \\ \mathbf{N}(\mathbf{X}_N) \end{bmatrix}, \qquad \mathbf{M}_d = \begin{bmatrix} \mathbf{M}_1 & \mathbf{0} & \ldots & \mathbf{0} \\ \mathbf{0} & \mathbf{M}_2 & \ldots & \mathbf{0} \\ \vdots & \vdots & \ddots & \vdots \\ \mathbf{0} & \mathbf{0} & \ldots & \mathbf{M}_N \end{bmatrix}, \qquad \mathbf{M}_i = \begin{bmatrix} M_i & 0 \\ 0 & M_i \end{bmatrix}.$$

The procedure of time integration of the dynamic equations is conditionally stable. It has been shown in [9] that the critical value of the time increment depends on the position of material points with respect to the position of the computational mesh. In the least advantageous situation, when there exists an element consisting of material points located closely to one edge, the critical time increment is much shorter than in the finite element method.

3.3. Time integration of constitutive relations

The explicit rule of time integration is used in the Kolymbas hypoplastic model, Equation (16), and for the pressure-volume change relation (14) used in the model applied to the problem of silo filling. In the case of elastic-perfectly plastic and elastic-viscoplastic relations, the fully implicit (backward Euler) rule is utilized (*e.g.* [26]). The details of the procedure related to the elastic-plastic model can be found in [9].

3.4. Solution to the frictional contact problem

As mentioned in Section 2.3 above, the penalty regularization method is utilized in the paper to solve the frictional contact problem. The relation between the normal components of velocity and contact stress need not be regularized, because in the

case of a non-cohesive granular material the inequality $\sigma_N \leq 0$ is always true and normal tractions at the nodes of the computational mesh can be calculated from the equations of motion by setting $v_N = 0$.

Unlike the constitutive relations which are satisfied at the material points, the relations pertinent to the contact phenomenon are fulfilled at the nodes of the computational mesh. The contact problem is relatively easy to solve for a mesh which is constant in time. The following algorithm of solving the frictional contact problem is applied.

For each node of the computational mesh, located on the surface of an obstacle body (silo walls), the normal contact force (at time $t+\Delta t$) is obtained from the relation:

$$F_{cN}^{t+\Delta t} = -F_N^{t+\Delta t} + R_N^{t+\Delta t},$$

which follows from the equation of motion (21) under the condition $a_N^{t+\Delta t} = 0$. Then, the following cases are considered:

I. Contact ($F_{cN}^{t+\Delta t} \leq 0$)

1. Sticking node
   The trial value of the tangential force is calculated from the equation:
   $$F^{\mathrm{e}} = F_T^t - c_T v_T^{t+\Delta t} \Delta t,$$
   where $c_T > 0$ is the penalty parameter.
   a) If $|F^{\mathrm{e}}| \leq \mu |F_N^{t+\Delta t}|$ then $F_T^{t+\Delta t} = F^{\mathrm{e}}$; the node is considered sticking in the next step.
   b) If $|F^{\mathrm{e}}| > \mu |F_N^{t+\Delta t}|$ then $F_T^{t+\Delta t} = (F^{\mathrm{e}}/|F^{\mathrm{e}}|)\mu |F_N^{t+\Delta t}|$; the node is considered sliding in the next step.
2. Sliding node
   a) If $v_t^t v_t^{t+\Delta t} > 0$, then $F_T^{t+\Delta t} = -(v_T^{t+\Delta t}/|v_T^{t+\Delta t}|)\mu |F_N^{t+\Delta t}|$ and the node is considered sliding in the next step.
   b) If $v_t^t v_t^{t+\Delta t} \leq 0$, then calculations are performed as for a sticking node, but the trial tangential force is expressed as follows:
   $$F^{\mathrm{e}} = -\frac{v_T^t}{|v_T^t|}\mu |F_N^{t+\Delta t}| - c_T v^{t+\Delta t} \Delta t.$$

II. Separation ($F_{cN}^{t+\Delta t} = 0$)
Set $F_{cT}^{t+\Delta t} = 0$. The node is considered sticking in the next step in the case of contact.

4. Numerical examples

Several discharge and filling problems are presented in this section. Plane and axisymmetric problems are considered for various constitutive models.

4.1. A discharge problem: plane flow

Plane flow in a silo, a cross-section of which is shown in Figure 2, is considered. The dimensions shown in the figure are given in centimeters.

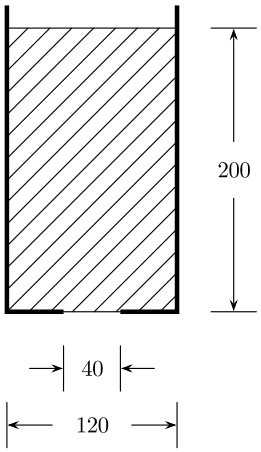

Figure 2. Cross-section of a silo: plane strain problem

Calculations have been made for the following values of mass density and angle of friction between granular material and silo walls: $\varrho = 1\,500\,\mathrm{kg/m^3}$, $\varphi_w = 20^\circ$, respectively. In the analysis, three constitutive models have been applied with the material data as follows:

- the elastic-perfectly plastic model with the Drucker-Prager yield condition: $E = 1 \cdot 10^6\,\mathrm{Pa}$, $\nu = 0.3$, $\varphi = 29.38^\circ$;
- the elastic-viscoplastic model with the Drucker-Prager yield condition: $E = 1 \cdot 10^6\,\mathrm{Pa}$, $\nu = 0.3$, $\varphi = 29.38^\circ$, $\gamma = 50\,\mathrm{s^{-1}}$, $N = 1$;
- the Kolymbas hypoplastic material model: $C_1 = -208.2$, $C_2 = 7.450$, $C_3 = 233.1$, $C_4 = -671.8$.

The initial (static) stress field has been found by the finite element method, assuming the gravity forces to be applied quasi-statically in 5 load increments. The computational mesh used in the calculations contains 3 011 nodes and 5 768 elements; 20 736 material points are introduced. The time increment applied in the explicit procedure of time integration of the dynamic equations has been set at $\Delta t = 1.25 \cdot 10^{-4}\,\mathrm{s}$.

The flow rate of the bulk material has been calculated; the results are shown in Figure 3.

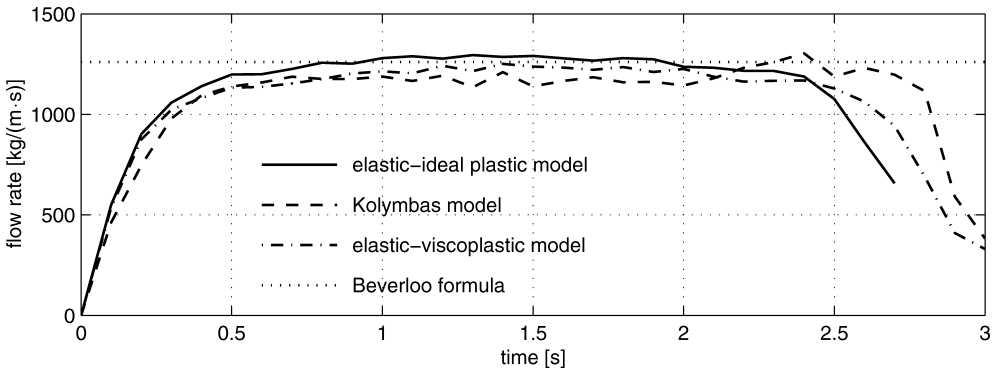

Figure 3. Flow rate diagrams

It can be noticed that the flow rate has stabilized after a short initial interval, which has been observed in experiments, see *e.g.* [27]. The value of flow rate, $W = 1\,261\,\mathrm{kg/(ms)}$, calculated according to the empirical formula by Beverloo *et al.* [27], is also indicated in the figure. The formula reads as follows:

$$W = 45\varrho A' \sqrt{g D_h'}, \tag{24}$$

where the flow rate, W, is measured in [g/min], A' denotes an effective area of the outlet in [cm^2], related to the effective hydraulic diameter, D_h' [cm]. The effective hydraulic diameter is expressed with the hydraulic diameter, D_h, and the grain diameter, d, as follows: $D_h' = D_h - 1.4d$. The above-mentioned value of the flow rate has been calculated after setting $d = 0$ in the latter equation.

Apparently, the elastic-viscoplastic material model yields a smaller value of flow rate than the elastic-perfectly plastic model. This follows from the fact that the elastic-viscoplastic model is a regularization of the elastic-perfectly plastic one; the latter can be regarded as the viscoplastic model with the viscosity parameter $\gamma = \infty$. The lowest flow rate has been obtained for the Kolymbas hypoplastic material model.

The flow patterns obtained for the considered material models are presented in Figures 4–6.

Considerable differences are observed in the flow patterns depending on the constitutive model. In the Kolymbas model, considerable shear deformations are observed in the upper part of the material during the initial stage of the flow, while nearly rigid motion is predicted for this stage by the other two constitutive models. As the discharge process advances, funnel flow is observed for the elastic-plastic models in contrast to the Kolymbas model, for which the flow is much smoother. Comparing the results from Figures 4 and 5, it can be noticed that the deformation field obtained for the viscoplastic material is smoother than that related to the elastic-perfectly plastic one, where the formation of two shear bands is visible (Figure 4, $t = 1.5\mathrm{s}$).

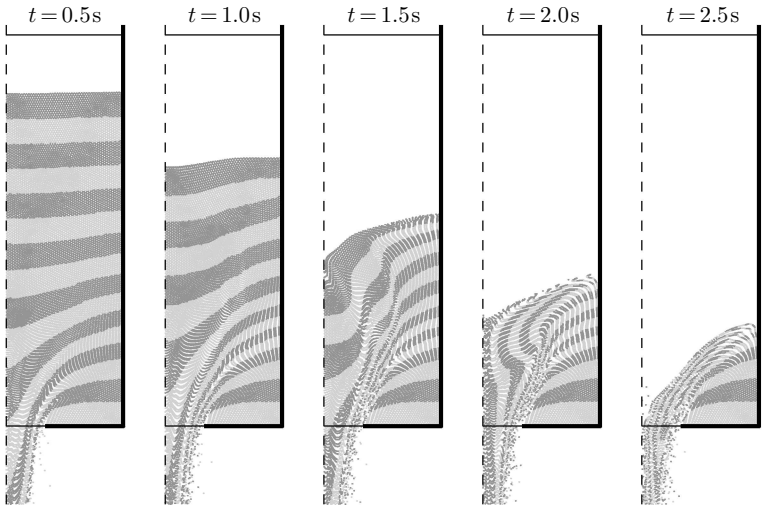

Figure 4. Flow pattern: plane strain problem, elastic-perfectly plastic model

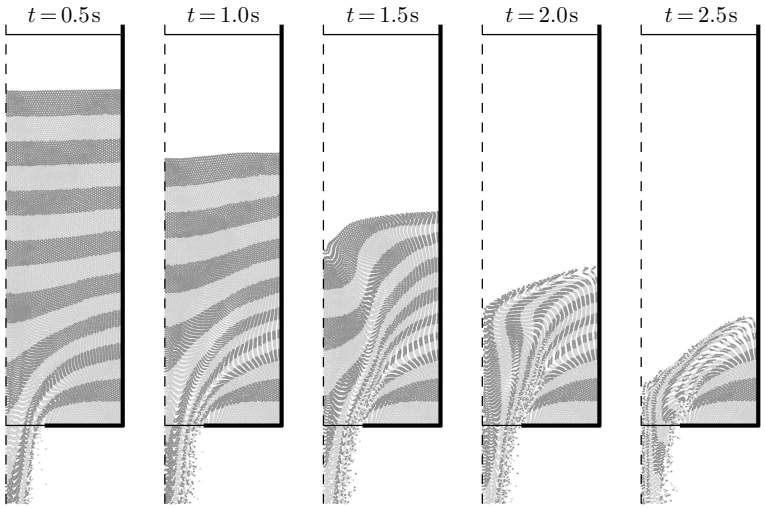

Figure 5. Flow pattern: plane strain problem, elastic-viscoplastic model, $\gamma = 50\text{s}^{-1}$

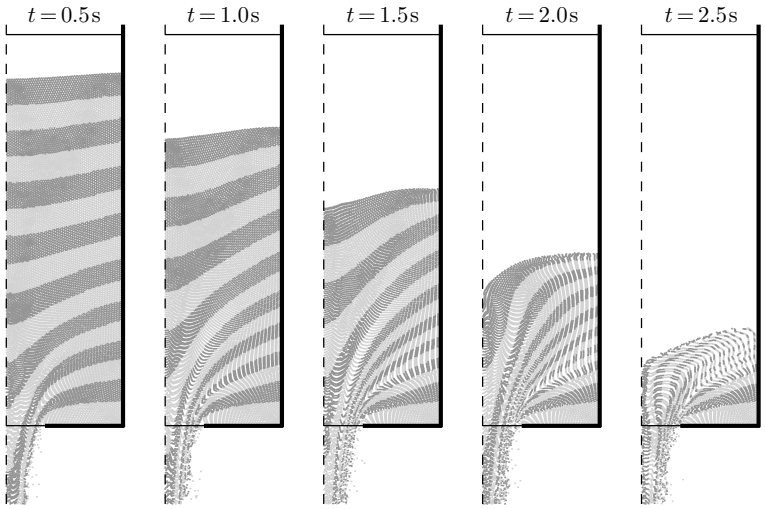

Figure 6. Flow pattern: plane strain problem, Kolymbas hypoplastic model

The diagrams of dynamic wall tractions, obtained for several instants, are shown in Figures 7–9. For comparison, a diagram of tractions calculated by the quasi-static analysis of the elastic-perfectly plastic material model is shown in Figure 10.

The normal and tangential tractions are drawn with thick and thin lines, respectively. The results obtained for the hypoplastic model differ considerably from those of the other two constitutive models; the largest differences appear on the vertical wall of the silo. It is interesting to notice the change of direction of tangential traction in the neighborhood of the cross-section's corner. This phenomenon is caused by unloading of the material remaining in the silo.

4.2. A discharge problem: axisymmetric flow

The discharge problem is considered for a cylindrical silo. A cross-section of the silo is shown in Figure 11, where dimensions are given in centimeters. Two variants

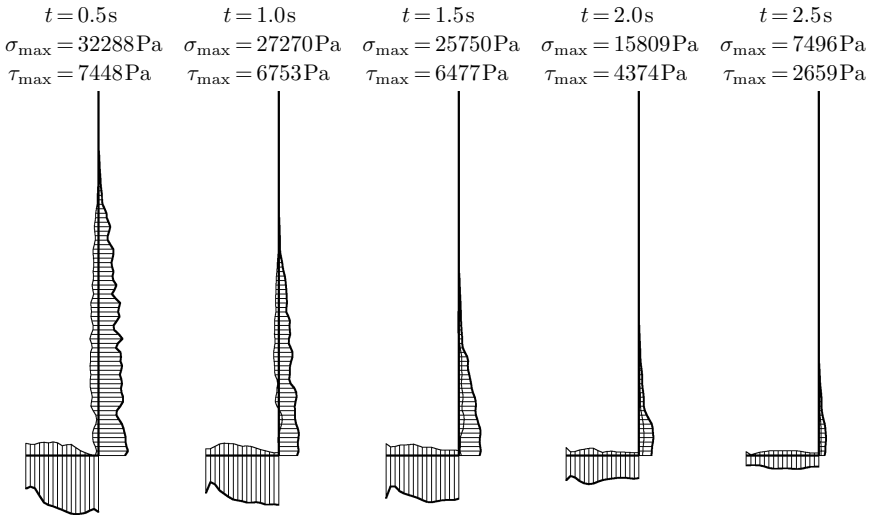

Figure 7. Wall tractions: plane flow, elastic-perfectly plastic model

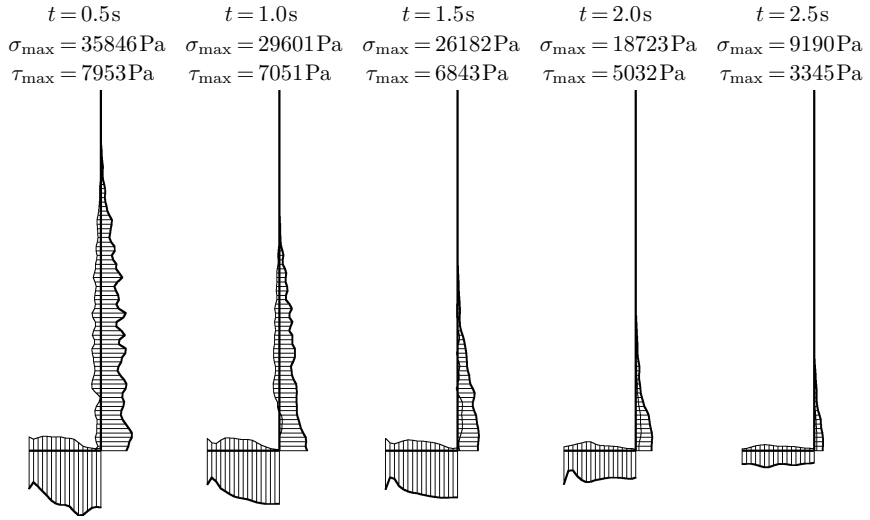

Figure 8. Wall tractions: plane flow, elastic-viscoplastic model, $\gamma=50\text{s}^{-1}$

of the flow are analyzed: for the silo with and without an insert controlling the flow pattern. Calculations are made for the elastic-plastic material model with the Drucker-Prager yield condition. The material data is as follows: Young's modulus $E=1\cdot10^6$ Pa, Poisson's ratio $\nu=0.3$, mass density $\varrho=1\,500\text{kg/m}^3$, the angle of internal friction $\varphi=29.38^\circ$, the angle of friction between the flowing material and silo walls $\varphi_w=20^\circ$.

In the case of the silo without an insert, a mesh of 9 818 elements with 5 080 nodes and 31 000 material points is introduced for one half of the silo cross-section. In the analysis of the silo with an insert, a mesh of 9 876 elements with 5 125 nodes, and 31 232 material points is applied for space discretization. The initial field of stresses has been calculated by the standard finite element method, assuming that the gravity forces are applied quasi-statically. The procedure of time integration of the dynamic equations has been performed with the time increment $\Delta t=2.5\cdot10^{-5}$s.

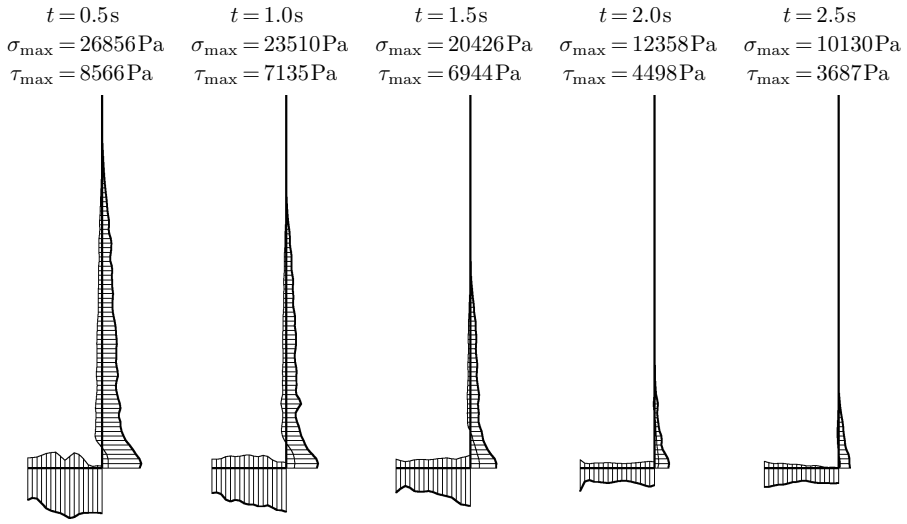

Figure 9. Wall tractions: plane flow, Kolymbas hypoplastic model

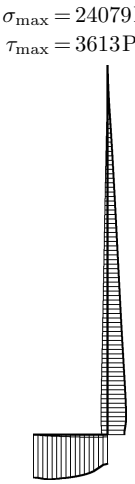

Figure 10. Initial wall tractions: quasi-static solution

The results of this analysis are shown in Figures 12 and 13 for the silo without and with the insert, respectively. Flow patterns and diagrams of wall tractions are shown in the figures. The normal and tangential tractions are depicted with thick and thin lines, respectively. Because of the symmetry, only the right half of the silo has been shown.

Comparing the obtained results, a difference in flow pattern is observed for the two analyzed cases. Funnel flow is obtained for the silo without the insert, while in the other case mass flow is observed in the region above the insert. A reduction of wall tractions is noticed in the neighborhood of the insert. It is visible that the direction of tangential tractions acting on the vertical wall in the vicinity of the corner (Figure 12) is changed due to unloading of the part of the granular material which remains in the silo. This phenomenon has been observed in experiments.

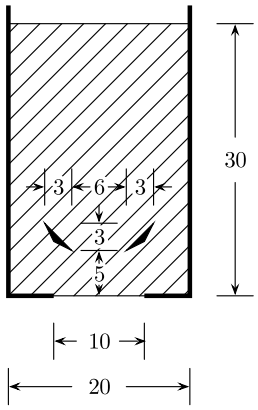

Figure 11. Cross-section of a cylindrical silo

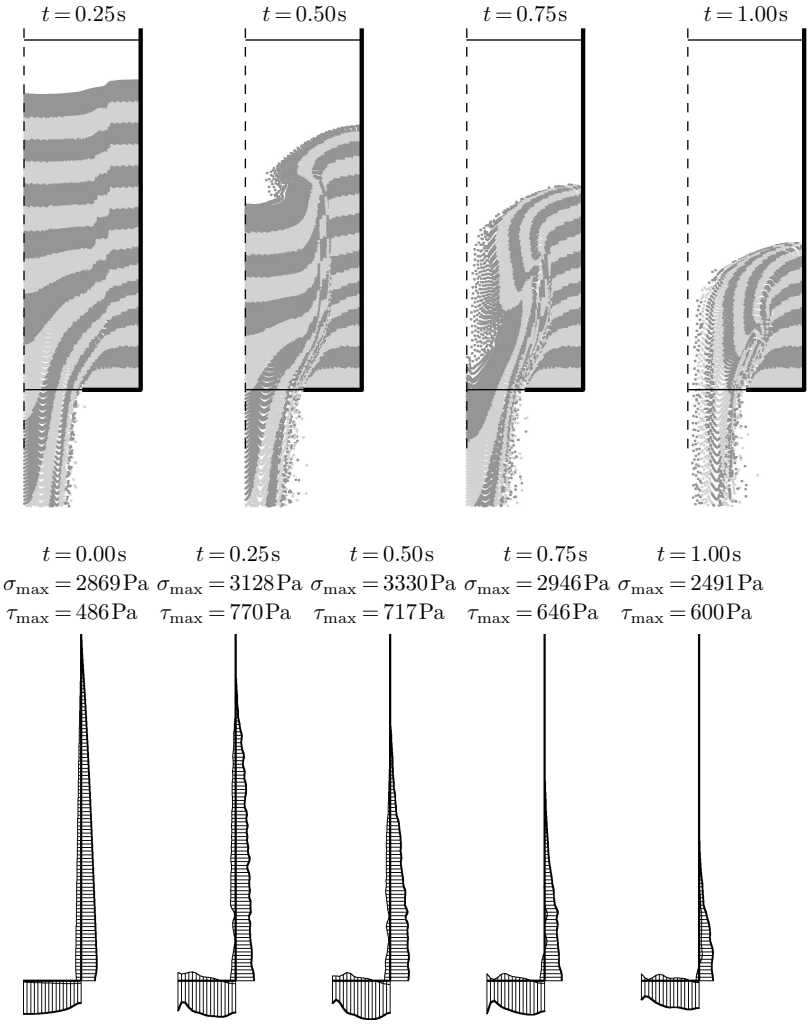

Figure 12. Flow pattern and wall tractions: cylindrical silo without insert

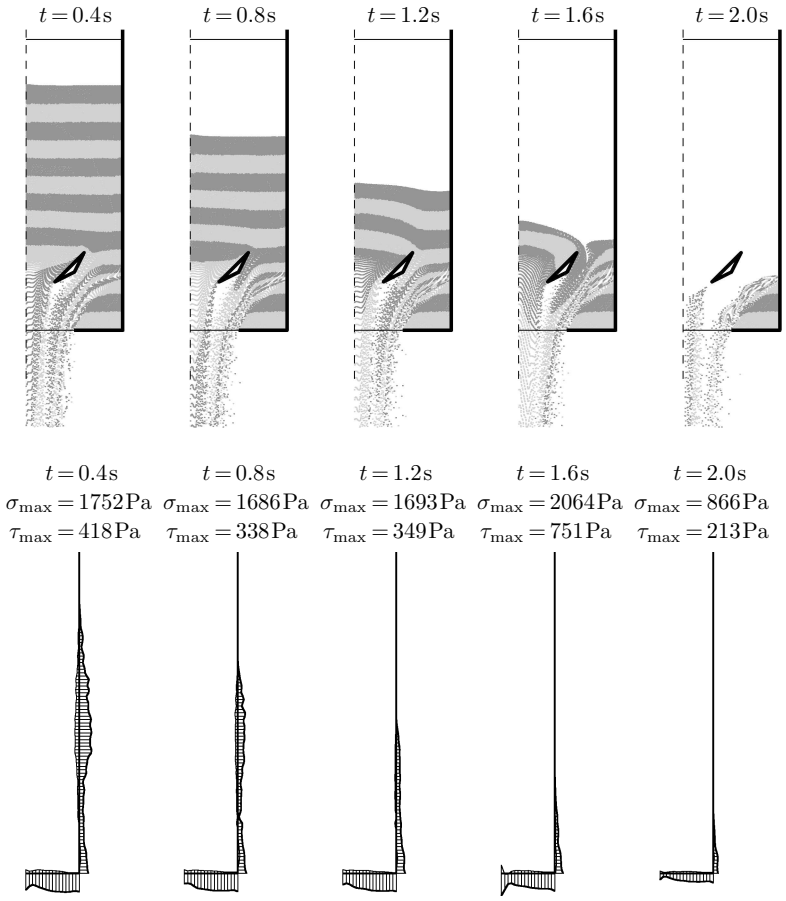

Figure 13. Flow pattern and wall tractions: cylindrical silo with insert

The results of the analysis show that the material point method can easily model such complicated phenomena as high distortions and self-contact of the granular material. In contrast to the material point method, the problem of flow of the granular material around an insert is very difficult to analyze by the finite element method formulated in the Lagrangian description of motion.

4.3. A discharge problem of the silo-in-silo type

Due to its ALE features, the material point method allows one to analyze granular flow for silos of complex shapes. An example of plane flow in a container of the silo-in-silo type, shown in Figure 14, has been considered. Calculations have been made with the same material data as used in the previous example.

The flow pattern is shown in Figure 15; much faster flow is noticed in the outer part of the silo than in the middle.

4.4. The filling problem

It is assumed that a silo is filled by releasing portions of granular material of given mass and volume with given frequency. The initial position of these portions is fixed in space; the initial velocity and stress fields are equal to zero. The released

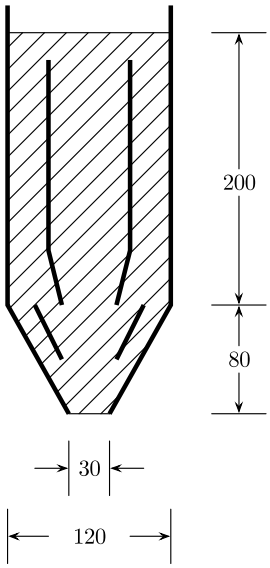

Figure 14. Silo-in-silo

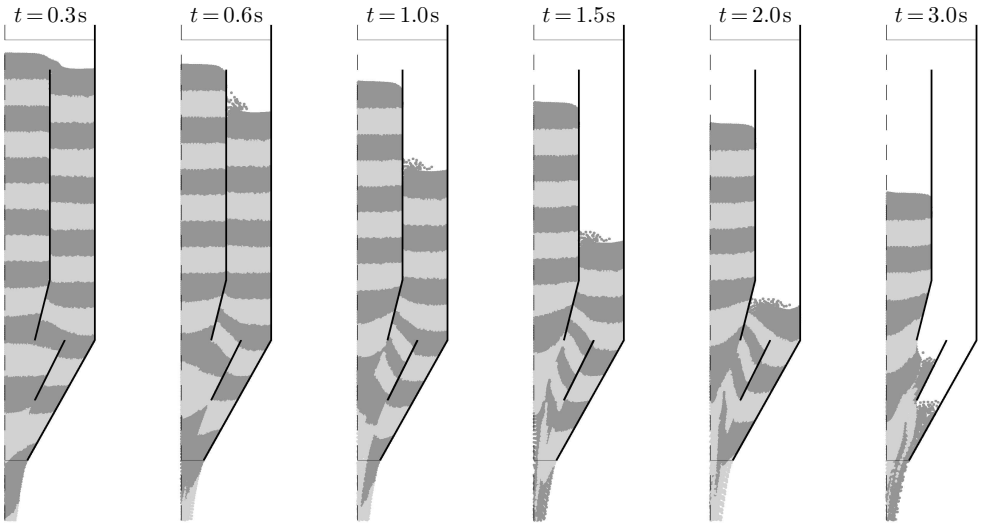

Figure 15. The silo-in-silo problem: flow pattern

material falls freely after the start and hits the bottom (wall) of the silo or the material stored in it.

The plane strain problem is solved for a silo the cross-section of which is presented in Figure 16, where dimensions are given in centimetres. It is assumed that each released portion of the granular material occupies cuboid region of $20 \times 10 \times 100$cm shown in Figure 16 and its mass is 20kg. The portions are released in 42s with the step set at 0.2s.

Calculations are made for the following material data: $\kappa = 0.02$, $\nu = 0.3$, $e_0 = 0.9$, $p_0 = 600$Pa, $\varphi = 30^\circ$, $\mu = 10^4$Pa·s, $\gamma = 10^4\,\mathrm{s}^{-1}$, $N = 1$, and mass density for the skeleton

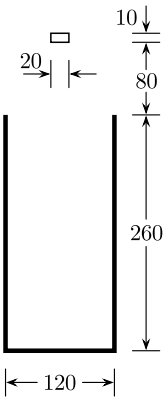

Figure 16. The filling problem: cross-section of the analyzed silo

$\varrho_s = 2850\,\mathrm{kg/m^3}$. It is assumed that the angle of friction between the granular material and silo walls is $\varphi_w = 20^\circ$.

Because of the symmetry, only a half of the cross-section of the silo has been analyzed. The total number of material points defined has been 30 240, while the number of points in each released portion has been 144 (12×12). The computational mesh has had 2 131 elements and 1 146 nodes. The problem has been solved with the time increment $\Delta t = 2 \cdot 10^{-5}\,\mathrm{s}$ applied in the explicit procedure of time integration of the dynamic equations.

The deformation history is presented in Figure 17, where each layer except the last contains 576 material points released in four consecutive portions.

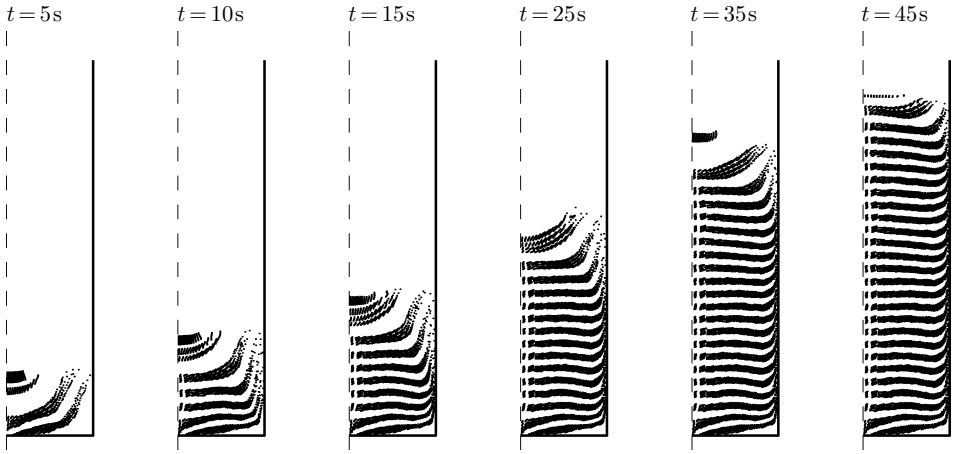

Figure 17. Phases of the filling process

Tractions between the granular material and the silo walls and bottom are shown in Figure 18 for the same time instants for which deformation is shown in the previous figure. The normal and tangential tractions are represented by the thick and thin lines, respectively. The results obtained for the last shown filling phase (45s) are compared with those evaluated by the quasi-static finite element analysis and presented in Figure 19. The largest differences are observed for the bottom of the silo.

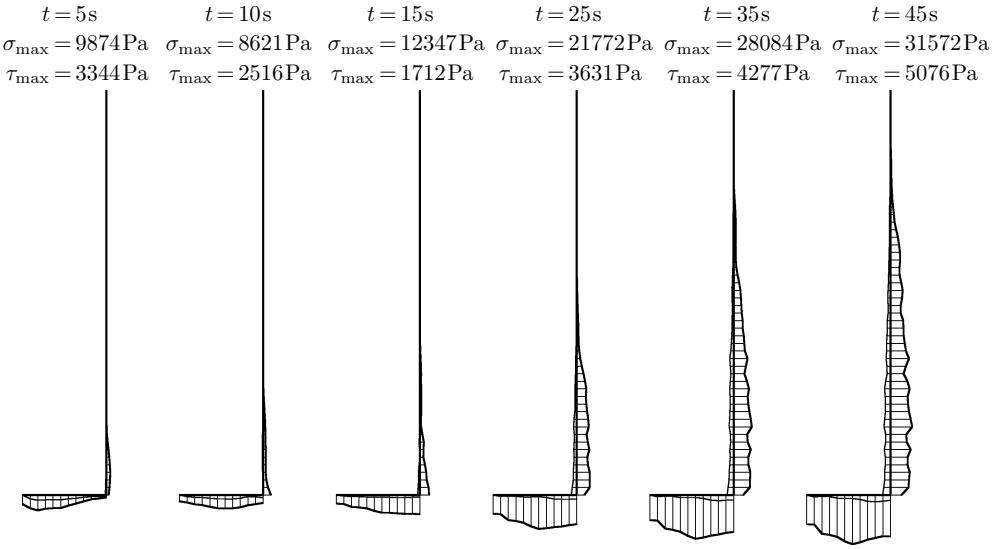

Figure 18. The silo filling problem: wall tractions

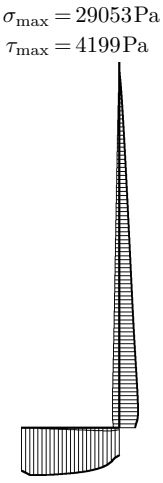

Figure 19. Wall tractions: quasi-static finite element solution

5. Conclusions

The material point method – a variant of the finite element method formulated in an arbitrary Lagrangian-Eulerian (ALE) description of motion – has been described in the present paper and applied to a large strain engineering problem of granular flow in a silo. The results shown in the paper prove that the method is a robust tool in the analysis of such complicated tasks as discharging and filling a silo. Some problems, like granular flow around a silo insert and the problem of self-contact of granular material, can be solved relatively easily by the material point method, in contrast to the standard finite element method formulated in the Lagrangian frame. The material point method seems to be very promising as a tool of analysis for other large-strain problems like the motion of avalanches and the simulation of earth-moving or plastic

forming processes (its application to the latter problem is given in [28]). However, the method is time consuming. It seems that the use of a parallel computation technique may reduce the time consumption of the method, as calculations performed at the level of material points and elements and the solution of the system of algebraic equations can be easily parallelized when a diagonalized mass matrix is utilized.

Acknowledgements

This work has been supported by the (Polish) State Committee for Scientific Research through the grant No. 7 T07A 006 17.

References

[1] Häussler U and Eibl J 1984 *J. Eng. Mech. ASCE* **110** 957
[2] Eibl J and Rombach G 1988 *Proc. 6th Int. Conf. on Numerical Methods in Geomechanics* (Swoboda G, Ed.), Balkema, pp. 317–320
[3] Runesson K and Nilsson L 1986 *Int. J. Bulk Solids Handling* **6** 877
[4] Elaskar S A, Godoy L A, Gray D D and Stiles J M 2000 *Int. J. Sol. Struct.* **37** 2185
[5] Więckowski Z and Klisiński m 1995 *Arch. Mech.* **47** 617
[6] Langston P A, Tüzün U and Heyes D M 1995 *Chem. Eng. Sci.* **50** 967
[7] Owen D R J, Feng Y T, Klerck P A, Yu J and Crook A J L 2001 *Proc. 2nd Europ. Conf. on Computational Mechanics ECCOMAS*, IACM, Cracow, CD-ROM
[8] Mühlhaus H-B, Sakaguchi H, Moresi L and Fahey M 2001 *Continuous and Discontinuous Modelling of Cohesive-Frictional Materials* (Vermeer P A, Diebels S, Ehlers W, Herrmann H J, Luding S and Ramm E, Eds), Springer, Berlin, pp. 185–204
[9] Więckowski Z, Youn S K and Yeon J H 1999 *Int. J. Numer. Meth. Eng.* **45** 1203
[10] Oger L, Savage S B Sayed M 2000 *Proc. 4th Euromech Conf.*, Metz pp. 126–126
[11] Harlow F H 1964 *Methods for Computational Physics* **3**, (Adler B, Fernbach S and Rotenberg M, Eds), Academic Press, New York, pp. 319–343
[12] Burgess D, Sulsky D and Brackbill J U 1992 *J. Comput. Phys.* **103** 1
[13] Sulsky D, Chen Z and Schreyer H L 1994 *Comp. Meth. Appl. Mech. Eng.* **118** 179
[14] Sulsky D, Zhou S-J and Schreyer H L 1995 *Comput. Phys. Commun.* **87** 236
[15] Sulsky D and Schreyer H L 1996 *Comp. Meth. Appl. Mech. Eng.* **139** 409
[16] Belytschko T, Krongauz Y, Organ D, Fleming M and Krysl P 1996 *Comp. Meth. Appl. Mech. Eng.* **139** 3
[17] Zienkiewicz O C and Taylor R L 2000 *The Finite Element Method* **1**, 5$^{\text{th}}$ Edition, Butterworth-Heinemann, Oxford
[18] Liu G R 2001 *Mesh Free Methods: Moving Beyond the Finite Element Method*, CRC Press
[19] Duvaut G and Lions J L 1976 *Inequalities in Mechanics and Physics*, Springer-Verlag, Berlin
[20] Kikuchi N and Oden J T 1988 *Contact Problems in Elasticity: A Study of Variational Inequalities and Finite Element Methods*, SIAM, Philadelphia
[21] Michałowski R and Mróz Z 1970 *Arch. Mech.* **30** 259
[22] Wriggers P, Vu Van T and Stein E 1990 *Computers & Structures* **37** 319
[23] Schofield A and Wroth C P 1968 *Critical State Soil Mechanics*, McGraw-Hill, New York
[24] Kolymbas D 1988 *Constitutive Equations for Granular Non-Cohesive Soils* (Saada A S and Bianchini G, Eds), Balkema, Rotterdam, pp. 349–359
[25] Kolymbas D 1991 *Ing. Arch.* **61** 143
[26] Zienkiewicz O C and Taylor R L 2000 *The Finite Element Method* **2**, 5$^{\text{th}}$ Edition, Butterworth-Heinemann, Oxford
[27] Beverloo W A, Leniger H A and van de Velde J 1961 *Chem. Eng. Sci.* **15** 260
[28] Więckowski Z 2002 *Proc. 5th World Congress on Computational Mechanics (WCCM V)* (Mang H A, Rammerstorfer F G and Eberhardsteiner J, Eds), Vienna University of Technology, Vienna, Austria, http://wccm.tuwien.ac.at/